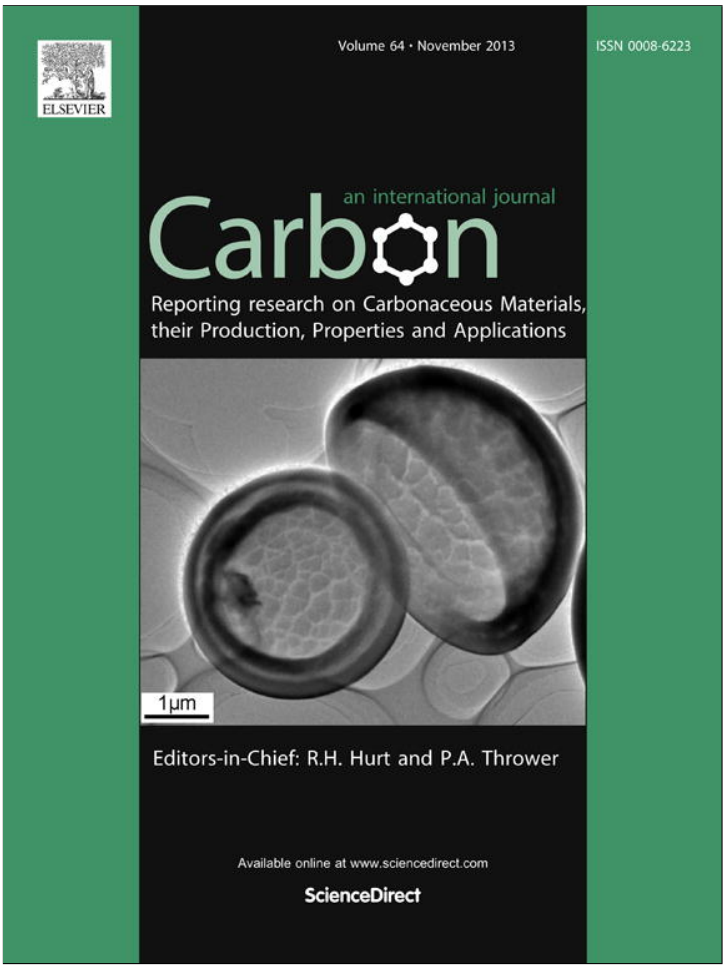

CARBON 64 (2013) 170–177

Available at www.sciencedirect.com

SciVerse ScienceDirect

journal homepage: www.elsevier.com/locate/carbon

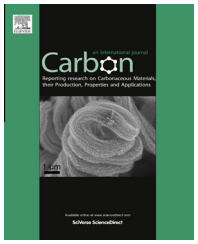

Carbon black cathodes for lithium oxygen batteries: Influence of porosity and heteroatom-doping

Yongliang Li [a], *Xifei Li* [a], *Dongsheng Geng* [a], *Yongji Tang* [a], *Ruying Li* [a], *Jean-Pol Dodelet* [b,*], *Michel Lefèvre* [c], *Xueliang Sun* [a,*]

[a] *Department of Mechanical and Materials Engineering, The University of Western Ontario, London, Ontario N6A 5B9, Canada*
[b] *INRS-Énergie, Matériaux et Télécommunications, 1650 Boulevard Lionel Boulet, Varennes, Québec J3X 1S2, Canada*
[c] *Canetique Electrocatalysis Inc., 1650 Boulevard Lionel-Boulet, Varennes, Québec J3X 1S2, Canada*

ARTICLE INFO

Article history:
Received 21 February 2013
Accepted 17 July 2013
Available online 24 July 2013

ABSTRACT

Carbon materials have been widely used as cathodes in lithium oxygen batteries but the detailed influence of the structure of these materials on their performance is not very clear yet. In this study, the same starting pristine commercial carbon black (N330) was treated under different atmospheres and the resultant carbons were employed as cathode materials for lithium oxygen batteries. It was demonstrated that the porosity and surface topology of these carbons tremendously changed as their treating time increased. The parameters that influenced the battery performance were identified. It was found that the main factor determining the battery performance is the specific surface area of the carbon mesopores, while nitrogen- or oxygen-bearing functionalities, introduced in these carbons during their heat-treatment or by contact with air after their pyrolysis, had little or no influence on the battery performance.

1. Introduction

Lithium oxygen battery is one of the most promising energy storage candidates for meeting the future demands of the electric vehicles (EVs) or hybrid electric vehicles (HEVs) [1,2]. However, the challenges for this battery system, such as the rate capability, cycle life, power performance, etc. should be overcome before lithium oxygen batteries can be used in practical applications [3]. It was reported that during discharge process of the battery, the product, Li_2O_2, deposits on the surface of the electrodes and eventually blocks the path ways for electrolyte and oxygen transportation, terminating the discharge process. Therefore, the electrodes are directly determining the battery performance.

To date, carbon materials are still the most studied cathode materials for lithium oxygen batteries, and efforts have been made to increase the oxygen solubility and diffusion, to decrease the accumulation of reaction products, and to create effective three-phase electrochemical interface of these materials [4–8]. For example, one-dimensional carbon materials (CNTs, CNFs) have been reported to exhibit good performance because they could form an interconnected porous electrode with high void volume [9,10]. Graphene nanosheets, a two-dimensional material showed significantly improvement for the battery performance due to its unique morphology and structures [11–13]. It was also reported that heteroatom-doping to carbon nanotubes and graphene nanosheets further increased the battery performance because of the active sites introduced into the pristine samples [14–16]. Due to abundance and low cost, carbon black has also been extensively studied as a cathode in lithium oxygen batteries. For example, several carbon black powders have been studied

* *Corresponding authors:* Fax: +1 450 9298198 (J.P. Dodelet); fax: +1 519 6613020 (X. Sun).
E-mail addresses: dodelet@emt.inrs.ca (J.-P. Dodelet), xsun@eng.uwo.ca (X. Sun).
0008-6223/$ - see front matter
http://dx.doi.org/10.1016/j.carbon.2013.07.049

by Xiao et al. [4] and the results suggested that the pore volume and the pore size affect the battery performance. Hall et al. [8] also suggested that electrode made of carbon aerogel with appropriate pore volume and pore diameter delivered high discharge capacity. The findings indicated that the limited discharge capacity was associated to pore clogging as claimed by others [17]. However, recently Luntz et al. [18,19] reported that the electrical passivation caused by the formation of discharge product layer on the electrode was the limiting factor by using the electrochemical experiments and modeling. They found that even a very thin layer (4–5 nm) of the insulated film of Li_2O_2 was sufficient to terminate the discharge reaction due to the increased electrical resistance at the electrode/electrolyte interface, then preventing further O_2 reduction. This would imply that the specific capacity should be related to the effective carbon surface area, accessible to the electrolyte and oxygen. In the present paper, various carbons all derived from the same starting commercial pristine carbon black (N330) were obtained by threating this carbon black in different treating atmospheres and for different times. The resulting carbons have been used as cathode in lithium oxygen batteries, revealing that the discharge capacity is proportional to the specific surface area of mesopores in these carbon electrodes. For the first time, the influence of various parameters resulting from the heat-treatment of the same starting carbon black, such as the content of disorganized carbon and heteroatom-doping effects, is studied in detail as well on the performance of the lithium oxygen battery.

2. Experimental

2.1. Sample preparation

Commercial N330 furnace carbon black (from Sid Richardson Carbon Corporation) was used as the starting material. It was heat-treated under NH_3 or CO_2 (with or without H_2) atmospheres. The percentage of mass that was lost during the heat-treatment, W, was calculated as follows:

$$W = \frac{\text{initial mass} - \text{final mass}}{\text{initial mass}} \times 100 \quad (1)$$

2.1.1. Samples treated by NH_3

500 mg of carbon black powder spread in a fused silica boat was pyrolysed in a fused silica reactor under NH_3 at 1050 °C until the desired mass losses (10%, 35%, 54%, 75%, 85%) were obtained. For the 75% and 85% mass losses, the samples were made with several pyrolysis to obtain around 150–200 mg of final powder.

2.1.2. Samples treated by CO_2 (with or without H_2)

500 mg of carbon black spread in a fused silica boat was pyrolysed in a fused silica reactor under CO_2 at 1050 °C until the desired mass losses (13%, 35%, 50%, 75%) were obtained. For the 75% mass loss, the sample was again made with several pyrolysis to obtain around 150–200 mg of final powder. These samples were further pyrolysed under H_2 at 950 °C to remove oxygen. It is possible that some oxygen was introduced in the sample by simple contact with air after pyrolysis.

2.2. Physical characterizations

The morphologies of the samples were characterized by Hitachi S-4800 field-emission scanning electron microscope (SEM) operated at 5.0 kV. N_2 adsorption/desorption isotherms were obtained using a Folio Micromeritics TriStar II Surface Area and Pore Size Analyser. The nitrogen and oxygen contents of the carbon materials were determined by Kratos Axis Ultra Al (alpha) X-ray photoelectron spectroscopy (XPS). Raman scattering (RS) spectra were recorded on a HORIBA Scientific LabRAM HR Raman spectrometer system equipped with a 532.4 nm laser.

2.3. Electrochemical measurements

Cathodes were prepared by casting a mixture of carbon materials and Polyvinylidene fluoride (PVDF) (Alfa Aesar) with a weight ratio of 9:1 onto a separator (Celgard 3500). The electrodes were 3/8 inch in diameter and the loadings were ~0.3 mg. Swagelok type cells composed of lithium foil anode, Celgard 3500 separator, different cathodes and a stainless steel mesh as current collector were used to carry out the electrochemical measurements. The electrolyte was 1 mol dm^{-3} $LiCF_3SO_3$ dissolved in Tetraethylene glycol dimethyl ether (TEGDME). The discharge/charge characteristics were performed by using an Arbin BT-2000 battery station in a 1 atm oxygen atmosphere at room temperature (25 °C).

3. Results and discussion

The morphology and the distribution of particle sizes of some samples resulting from the heat-treatment of N330 in NH_3 are shown in Fig. 1. The distribution of particle sizes of the carbon black was obtained from the analysis of SEM micrographs based on about 300 particles. It can be seen that the shape of the particles is kept almost the same, even after a loss of 75% of the pristine N330 carbon mass. However, the particle size is decreasing after the heat treatment. Several large particles (>40 nm) are observed at 0% mass loss but their number decreases at 75% mass loss, while the mean diameter of the maximum number of particles shifted from an initial value of 40–45 nm, at 0% mass loss, to 25–30 nm after 75% mass loss.

It is known that NH_3 etches the carbon black at 1050 °C according to the following reactions [20]

$$C + NH_3 \rightarrow HCN + H_2 \quad (2)$$

$$C + H_2 \rightarrow CH_4 \quad (3)$$

The gasification reactions of carbon blacks results in decreasing particle sizes and the occurrence of porosity leading to an increasing specific surface area of the remaining carbon black.

Fig. 2 shows the voltage profiles of initial discharge–charge cycle of lithium oxygen batteries employed carbon blacks with different mass losses as cathode materials at a current density of 75 mA g^{-1}. Both the discharge and charge specific capacities increase with the mass loss of carbon black increases and the values are summarized in Table S1. For instance, a discharge capacity of ~1062 mAh g^{-1} with a

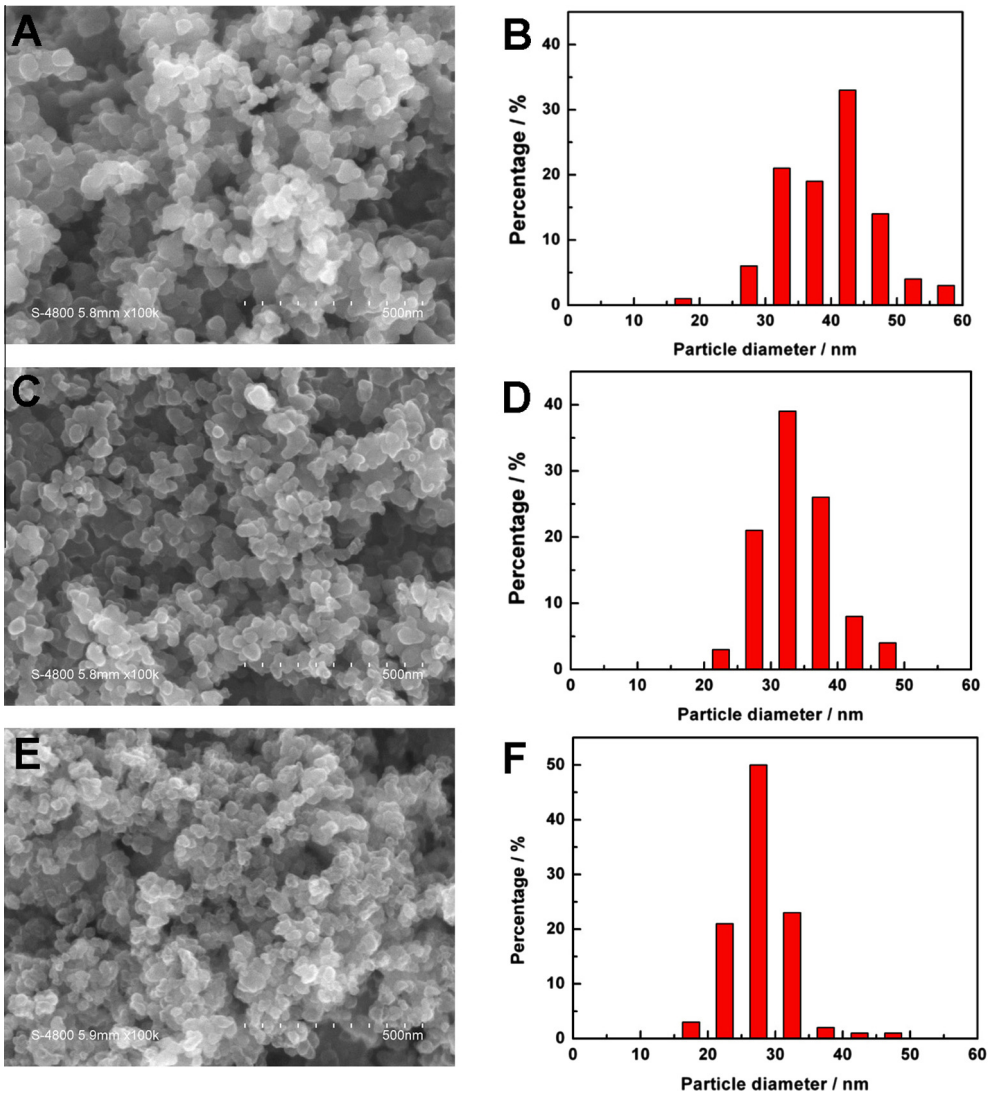

Fig. 1 – SEM images and particle size distributions of carbon blacks with mass loss of (a, b) 0%, (c, d) 35%, and (e, f) 75%.

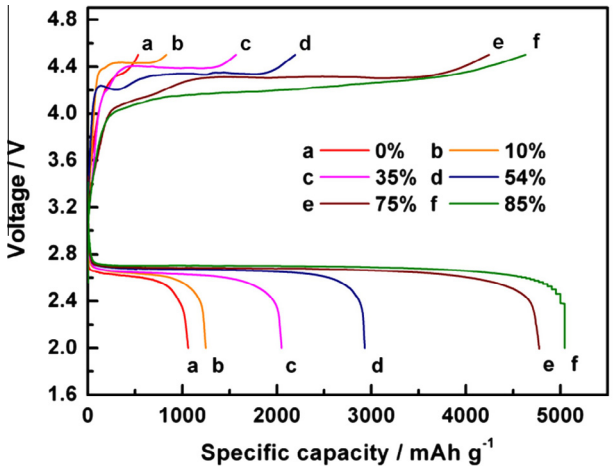

Fig. 2 – The first discharge–charge voltage profiles of lithium–oxygen batteries containing carbon blacks with different mass losses as cathode materials.

nominal discharge voltage of ~2.56 V was observed for the pristine sample (0% mass loss) while the charge capacity is ~533 mAh g^{-1} and nominal charge voltage is ~4.37 V. Also a discharge capacity of ~5045 mAh g^{-1} with a nominal discharge voltage of ~2.67 V was observed for the sample with a 85% mass loss, while the charge capacity is ~4631 mAh g^{-1} and nominal charge voltage is ~4.21 V. It is also noticed that the electrode polarizations decrease as the mass loss increases (from 1.81 V at 0% mass loss to 1.54 V for 85% mass loss; last column in Table S1).

The total specific surface area, the specific surface areas of micro-, meso-, and macro-pores of the samples have been measured as a function of mass loss. These results are presented in Fig. 3a. It can be seen that the total specific surface area and the mesopore surface areas of the samples both steadily increase as the mass loss increases. This behavior is different from that of the specific surface area of the micropores, which first increases, reaches a maximum, and then decreases as the mass loss increases. A formation mechanism of the porosity in carbon blacks has been well described by Jaouen et al. [21,22]. According to these authors,

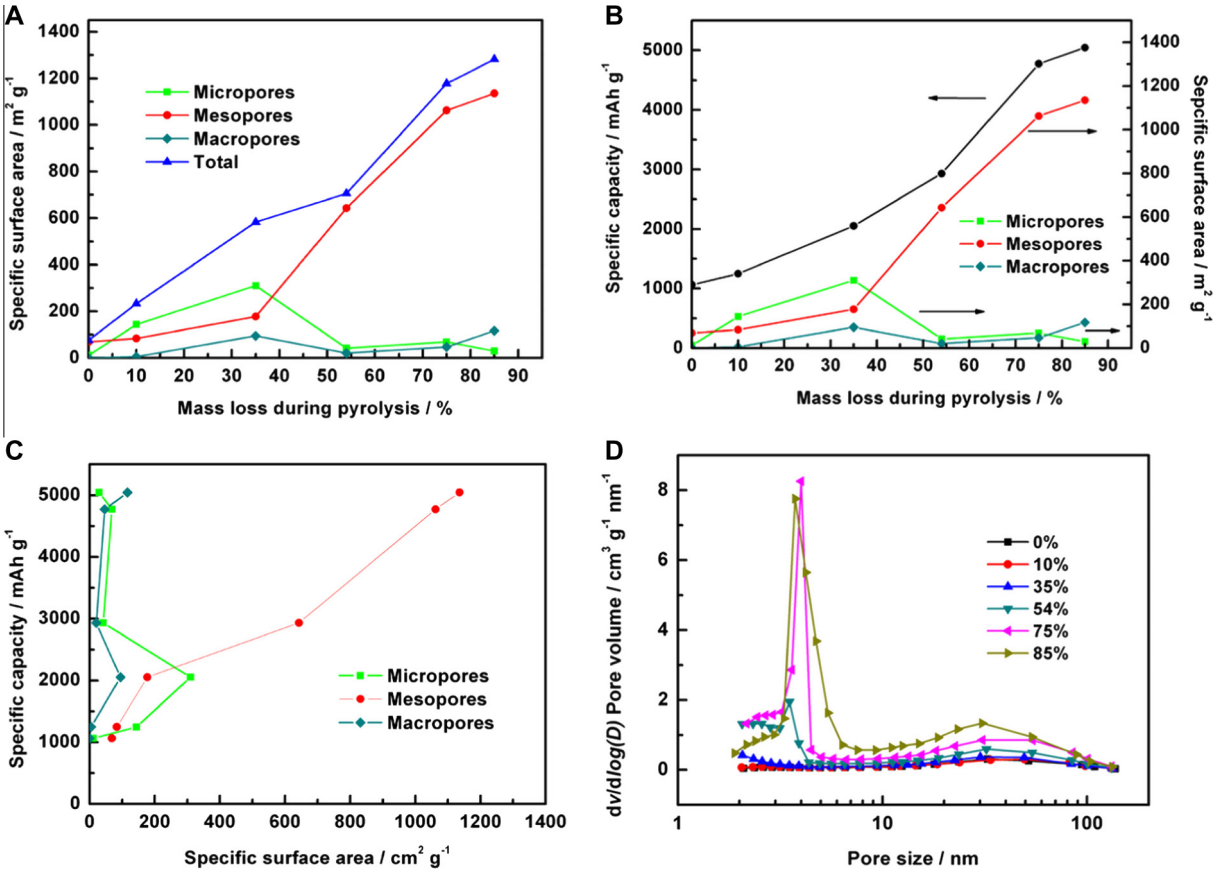

Fig. 3 – (a) Total specific area (BET) and specific surface areas for micropores, mesopores, and macropores vs. mass loss, (b) discharge capacity (left Y axis), the specific area of micropores, mesopores, and macropores (right Y axis) vs. mass loss during pyrolysis, (c) discharge capacity vs. the specific area for micropores, mesopores, and macropores and (d) the pore size distribution (PSD) curves for carbon blacks with various mass losses.

the surface area of the pristine carbon black is only that of the outer spheres of the carbon particles with almost no pores; then, as gasification of carbon proceeds according to Eqs. (2) and (3), disordered carbon is removed from the outer surface and some edge surface is created. As more disordered carbon is removed from the particle, the micropores become larger in size and deeper in length leading to the formation of mesopores. The surface area of mesopores increases as the treating time increases. It has been reported that the catalytic activity of Fe/N/C catalysts used for oxygen reduction reaction at the cathode of proton exchange membrane (PEM) fuel cells is related to the microporosity of their carbon black support, since their most active sites are hosted in these micropores [23,24]. However, in our case, it can be seen in Fig. 3b (right Y axis) that, for lithium oxygen batteries, only the specific surface area of mesopores vs. mass loss curve well matches the behavior of the discharge specific capacity vs. mass loss curve (Fig. 2b, left Y axis). This indicates that the surface area of mesopores plays the major role in determining the battery discharge performance. The correlation between discharge capacity and specific surface areas is further illustrated in Fig. 3c, where it is indeed shown that the discharge capacity only increases nearly linearly with an increase of the surface area of the mesopores.

Fig. 3d shows the pore size distribution (PSD) curves of carbon blacks with different mass losses. As can be seen, for the pristine carbon black, only the pores centered at size of ~30 nm are present. They are probably voids between the carbon black particles. Even when the mass loss increases to 35%, the volume of pores having sizes between 2 and 4 nm only slightly increases, while the volume of pores having sizes centered at ~30 nm remains almost the same. It has been reported that the discharge product, Li_2O_2, would not deposit in micropores because the electrolyte could not have access to them [7]. Therefore, the discharge product would deposit on the surface of the voids between carbon particles. When the mass loss reaches 54%, not only a peak at ~3.5 nm appears in Fig. 3d, but also the volume of the pore sizes in the range of 10–50 nm increases, as a result to the enlargement of micropores. As the pyrolysis time increases, the pore volume peaks at a pore size of ~3.8 nm, indicating that this is the main pore size in such carbon black when the mass loss is 75%. As expected, the volume of the pore with sizes of 10–50 nm continues to increase in these conditions. When the mass loss increases from 75% to 85%, the volume of pore size at ~4 nm does not increase anymore, but the volume of pore sizes from 10–50 nm increases a lot. This should be beneficial for discharge product accommodation. However, it can be

seen in Fig. S1 that the discharge capacity only slightly increases (~6%), while the volume of mesopores increases by more than 50%. From this observation, one may suggest that the very large increase in the volume of mesopores, when mass loss increases from 75% to 85%, is not more effective for accommodating discharge product deposition.

Recent studies have shown that oxygen reduction reaction kinetics in lithium air battery system is not a catalyzed reaction while the increase of discharge voltage is resulting from the increased amount of defects at the surface edge structure on carbon [25]. The charge process, which involves the decomposition of discharge product Li_2O_2, is expected to be governed by much slower kinetic than discharge process and the decreased charge voltage could be due to the electrical conductivity of electrode surface [26]. The cycle performance of the batteries employed carbon blacks with different mass losses at a current density of 300 mA g^{-1} is shown in Fig. S2. As can be seen, all the samples deliver reasonably high discharge capacity for the first cycle; however, the capacities decay rapidly after only a few cycles which are accompanied by increased in the polarization, mainly attributed to the rise in the electrode resistance as we discussed above. In addition, the reaction between Li_2O_2 with carbon and electrolyte during charge (>3.5 V) would also increase the electrode overpotential due to the formation of Li_2CO_3 [27,28]. Therefore, it is necessary to explore new approaches to reduce the charge potential, and recently, Bruce et al. reported that lithium air cell contained a redox-mediating molecule, tetrathiafulvalene (TTF), were cycled 100 times with complete reversibility of Li_2O_2 formation/decomposition on each cycle, and the charge voltage is less than 3.5 V [29]. Another possible solution is to apply a carbon-free cathode for lithium oxygen battery. Zhou et al. have suggested that the carbon-free cathodes should have high conductivity and no catalytic activity for electrolyte decomposition during discharge/charge processes, high stability toward oxygen radicals and not reactive with Li^+ in the working window [30]. An issue should also be considered is the dehydrofluorination of PVDF (a typical binder used in lithium oxygen battery) caused by the reaction with the intermediate discharge product, LiO_2, which reduces the discharge and charge capacities [31]. Furthermore, the electrode structure will change progressively due to the decomposition of binder, affecting the cycle performance.

While some of the pores are clogged as discharge product forms, passivation is the main issue for the cathode due to the low electrical conductivity of Li_2O_2. The actual nucleation-growth of Li_2O_2 on electrode should be somewhat complicated and it has been reported that the morphologies of the final products are varied from one carbon material to another. For example, disc-like and toroid-like shapes of Li_2O_2 particles were observed on carbon nanotube electrode [32]. Li_2O_2 nanorods and nanosheets were found on the sulphur-doped graphene nanosheet electrode [16]. There must be some variations in the thickness of the electrochemical deposition, i.e., generally the crystals prefer to grow at kink or step sites where the adspeciesare more stable. However, no matter how the crystal growth occurs, the electron-transport-limited reaction will take place at the interface of solid discharge product and carbon. Therefore, it is meaningful to estimate the thickness of Li_2O_2 on carbon electrode after battery discharge [33]. Shao-Horn and Gasteiger et al. have reported that 260 μC cm^{-2} carbon is the estimated normalized discharge which is corresponding to the deposition of one monolayer of Li_2O_2 on carbon black, and the number of monolayers of discharge products for our carbons can be estimated consequently [34,35]. The discharge capacity based on carbon mass can be expressed to the surface-normalized discharge capacity based on the specific area of the mesopores. It is shown in Table 1, that the sample with 10% mass loss has a surface-normalized discharge capacity very similar to that of pristine carbon (~5500 μC cm^{-2}). As the mass loss increases to 35%, the capacity decreases to 4158 μC cm^{-2} and the thickness of discharge product decreases from ~7 to ~5 nm accordingly [36]. The reason for the decreasing thickness of discharge products on carbon samples may be due to the different cathodic polarization of the carbon surface caused by the various surface-normalized currents (last column in Table 1) [37]. It is important to note that when the mass loss is more than 54%, the capacity values drop to 1600–1650 μC cm^{-2} for these samples; these values suggest that about six monolayers of Li_2O_2 are formed on the carbon surface, corresponding to a ~2 nm thick layer. It is expected that only a thin layer of product can stop the discharge reaction, which supports the hypothesis proposed by Luntz et al. [18,19]. As can be seen from Fig. 4, the estimated thickness of discharge product on carbon surface is smaller than the average pore size of each sample, suggesting that a too large pore size in the mesoporous range leads to a less efficient use of mesopore volumes, which is consistent with our observations described above. Fig. S3 shows the curve of discharge specific capacity vs.mesopore size. One can see that when the pore size is about 3.5 nm, the capacity is maximum, indicating that it is the desired pore size considering the passivation.

So far, we have shown that the specific surface area of carbon black mesopores is an important factor determining the lithium oxygen battery performance. These mesopores were obtained by pyrolysing N330 in NH_3 at 1050 °C. Now, it will be shown that similar results are also obtained when the porosity in N330 is generated by pyrolysing at 1050 °C the same carbon black in CO_2 (or $CO_2 + H_2$; to remove at least partially the oxygen-bearing functionalities introduced by the pyrolysis under CO_2). Indeed, as seen in Fig. S4, both groups of samples show that the specific surface areas of mesopores are also proportional to the discharge capacities. The pore size distribution curves are shown in Fig. S5 and it can be seen that all the curves steadly shift upwards for pore volumes in the small and large pore diameter regions. However, the amount of pores of which size at ~3.8 nm is relatively less in the carbon blacks refer to the pores in the diameter range of 10–50 nm. From Table S2, similar results about the deposit of discharge products as a thin film are also demonstrated for the carbon blacks treated by CO_2 with/without H_2, and the thickness of discharge products is very similar to that of the carbon samples treated by NH_3, especially at the mass losses are more than 40% (Fig. S6).

Raman spectroscopy is a powerful technique to identify the structure of carbon blacks. Fig. 5a and Fig. S7 show the Raman spectra of the NH_3-treated samples. Each spectrum was deconvoluted into five peaks as suggested by Sadezky et al.

Table 1 – Surface-normalized discharge capacity and current, and the corresponding number of Li_2O_2 monolayers deposited on the surface of mesopores for carbon blacks with different mass losses.

Mass loss/%	Surface-normalized discharge capacity/μC cm^{-2}	Number of monolayers	Surface-normalized current/μA cm^{-2}
0	5577	21.5	0.328
10	5349	20.6	0.268
35	4158	16.0	0.127
54	1641	6.3	0.035
75	1617	6.2	0.021
85	1600	6.2	0.020

[38]. The D band (~1365 cm^{-1}) and G band (~1590 cm^{-1}) correspond to disordered and graphitic carbon phase, respectively.

The peaks at about 1190, 1530, and 1620 cm^{-1} are associated with the sp^3 carbon, amorphous carbon, and another band accounting for structural disorder, respectively. The width at half maximum (FWHM) of the D band, W_D, in the Raman spectroscopy of the carbon black indicates the degree of structural disorder in the samples [39]. As can be seen from Fig. 5b, W_D decreases from 200 to 118 cm^{-1} as the mass loss increases from 0 to 85%. The constant decrease of the W_D clearly indicates the decrease of the amount of disordered carbon phase in the samples. Fig. 5c depicts the discharge specific capacity vs. W_D; it is obvious that the capacity increases as the amount of disordered carbon phase decreases in the carbon black. This finding is interesting because in our previous study about graphene nanosheets, the electrode made of nitrogen doped graphene nanosheets which have more defects delivered higher discharge capacity than pristine sample [12,13,15]. In this study, we believe that the different behavior comes from the nature of the carbon black and graphene nanosheets. A model for heat treatment of carbon blacks under NH_3 has been proposed by Jaouen et al. [27,28] and is shown in Fig. S8. The pristine carbon black particle has no pores and consists of disordered carbon and graphitic crystallites. Both disordered carbon and graphitic crystallite edges contribute to the D band in the Raman spectrum. At the beginning of the heat treatment, NH_3 only reacts with the outer surface of the disordered carbon, and it will take time t_c to remove all the disordered carbon from shell 1, thus micropores are created. However, as the heat treatment continues, NH_3 reacts not only with the disordered carbon on shell 2, but also with the edges of the graphitic crystallites on shell 1. It was found that, at 950 °C, NH_3 reacts about ten times faster with disordered carbon than with graphitic crystallites. As carbon black reaction with NH_3 proceeds, the microporous surface area increases therefore rapidly, but

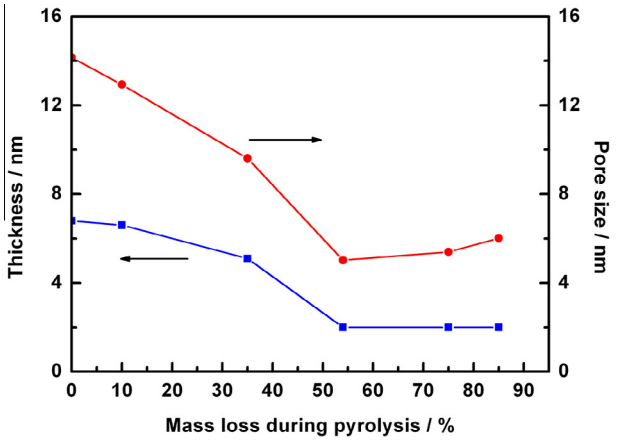

Fig. 4 – Estimated thickness of the discharge product on the surface (left Y axis) and pore size (right Y axis) of carbon blacks with different mass losses.

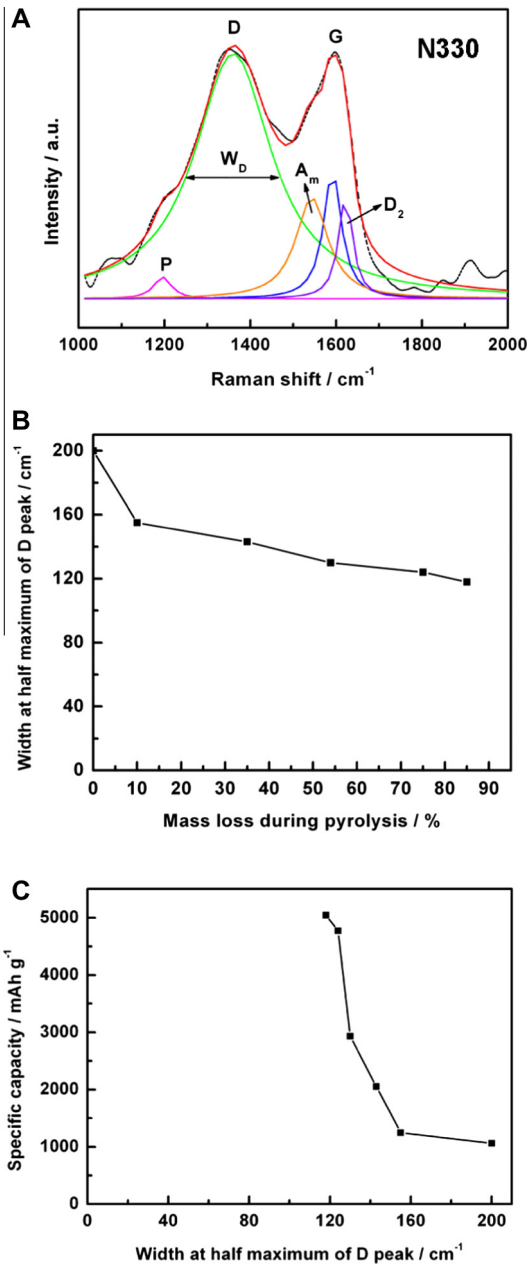

Fig. 5 – (a) Raman spectrum of the N330 carbon black, (b) Width at half maximum (FWHM) of D peak of carbon blacks vs. mass loss, and (c) the specific capacity vs. the fwhm.

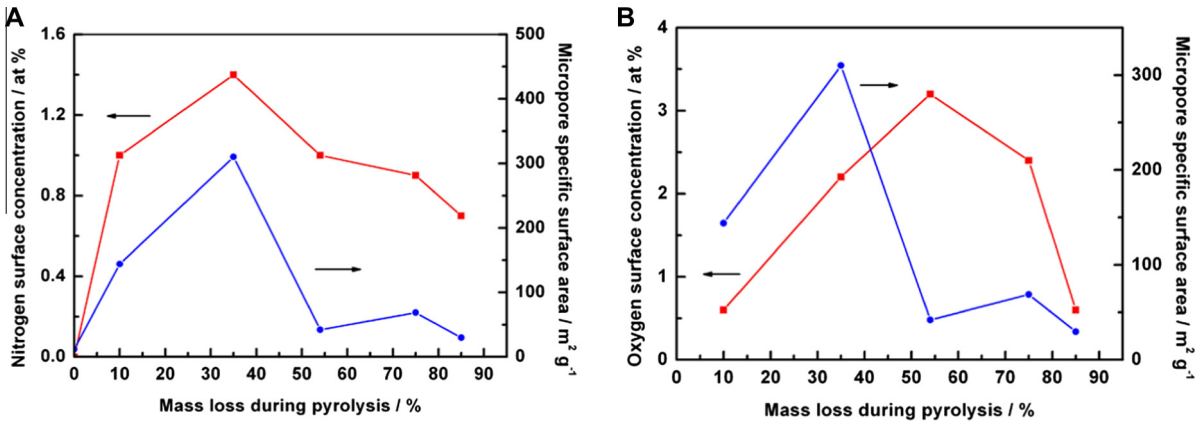

Fig. 6 – (a) Nitrogen surface concentrations (left *Y* axis), and (b) oxygen surface concentrations (left *Y* axis), the specific area of the micropores (right *Y* axis) of the carbon blacks with different mass losses.

the obtained micropores become larger at a slower rate. It is important to notice that, at certain time, the outmost graphitic crystallite layer will vanish, leading to a decrease in the particle diameter, and the micropores in that layer will vanish as well. From the calculations made with this model, it is predicted that, in a carbon black like N330, the surface area of micropores will increase from 0 to 30–35% mass loss, and then decrease (from mass loss >40%). The prediction matches very well our experimental results as shown in Fig. 3a. Due to the decreased amount of disordered carbon, W_D will continue to decrease as the treating time increases, however, the relative amount of edges of the graphitic crystallites to disorder carbon increase then, resulting in increasing battery discharge voltage, which is consistence of our finding above.

This work also enabled us to study the correlation (if any) between the nitrogen content of the carbon pyrolysed in NH_3 and the battery performance since nitrogen doping into the carbon framework and the occurrence of N-bearing functional groups has already been reputed to have a favorable influence on the performance of lithium oxygen batteries [14–16]. Fig. S9 shows the XPS survey spectra of the carbon blacks as the mass loss increased. As can be seen, nitrogen atoms were successfully doped into carbon blacks and the presence of oxygen may also be noticed at various amounts after the heat-treatments in NH_3 (Fig. 6). It is obvious that nitrogen content also follows the same trend as the microporosity vs. mass loss, that is it increases from 0 to 30–35% mass loss, and then decrease for mass loss >40%. Most of the nitrogen atoms are therefore located in the micropores. As these micropores have little influence on the performance of lithium oxygen batteries, the nitrogen doped sites are therefore not effective for improving battery performance (Fig. 6a).

Experimental results and density functional theory (DFT) calculations have shown that oxygen-containing functional groups on graphene electrode play an important role for battery performance [13]. However, it can be seen in Fig. 6b that the oxygen-bearing functional groups here also have no influence on the battery performance. The maximum of the oxygen surface concentration occurs at 54% mass loss, out of phase with the development of the microporous surface area, and simply decreases for mass losses larger than 54%, while the specific capacity of the carbon material continues to rise with the development of the mesoporous surface area.

4. Conclusions

In summary, commercial carbon black (N330) was treated under various atmospheres (NH_3, CO_2 and CO_2/H_2). The mesopore surface areas increased as the treating time increased while the micropore surface area only increased until the mass loss reached 35% and then decreased. It is suggested that the surface area of mesopores plays an important role for the discharge capacity of lithium oxygen batteries due to the passivation effect of discharge product film on the carbon surface. Nitrogen and oxygen-containing functional groups introduced by the gas treatments or by contact of the pyrolysed product with air, have very little or no influence on the performance of these carbon materials in lithium oxygen batteries. However, too large pore size in the mesoporous range leads to a less efficient use of mesopore volumes and the the desired pore size is about 3.5 nm considering the passivation effect. These findings established a correlation between the structure of carbon black and battery discharge capacity, which provides new insights into further designing or optimizing electrode materials for lithium oxygen batteries.

Acknowledgements

This research was supported by Natural Sciences and Engineering Research Council of Canada, Canada Research Chair Program, Canada Foundation for Innovation, Ontario Early Researcher Award and the University of Western Ontario.

Appendix A. Supplementary data

Supplementary data associated with this article can be found, in the online version, at http://dx.doi.org/10.1016/j.carbon.2013.07.049.

REFERENCES

[1] Abraham K, Jiang Z. A polymer electrolyte-based rechargeable lithium/oxygen battery. J Electrochem Soc 1996;143(1):1–5.

[2] Girishkumar G, McCloskey B, Luntz A, Swanson S, Wilcke W. Lithium–air battery: promise and challenges. J Phys Chem Lett 2010;1(14):2193–203.

[3] Lu Y, Kwabi D, Yao K, Harding J, Zhou J, Zuin L, et al. The discharge rate capability of rechargeable Li–O_2 batteries. Energy Environ Sci 2011;8(4):2999–3007.

[4] Xiao J, Wang D, Xu W, Wang D, Williford R, Liu J, et al. Optimization of air electrode for Li/air batteries. J Electrochem Soc 2010;157(4):A487–92.

[5] Williford R, Zhang JG. Air electrode design for sustained high power operation of Li/air batteries. J Power Sources 2009;194(2):1164–70.

[6] Yang X, He P, Xia Y. Preparation of mesocellular carbon foam and its application for lithium/oxygen battery. Electrochem Commun 2009;11(6):1127–30.

[7] Zhang S, Foster D, Read J. Discharge characteristic of a non-aqueous electrolyte Li/O_2 battery. J Power Sources 2010;195(4):1235–40.

[8] Mirzaeian M, Hall P. Preparation of controlled porosity carbon aerogels for energy storage in rechargeable lithium–oxygen batteries. Electrochim Acta 2009;54(28):7444–51.

[9] Mitchell R, Gallant B, Thompson C, Shao Horn Y. All-carbon-nanofiber electrodes for high-energy rechargeable Li–O_2 batteries. Energy Environ Sci 2011;8(4):2952–8.

[10] Zhang G, Zheng J, Liang R, Zhang C, Wang B, Hendrickson M, et al. Lithium–air batteries using SWNT/CNF buckypapers as air electrodes. J Electrochem Soc 2010;157(8):A953–6.

[11] Li Y, Wang J, Li X, Geng D, Li R, Sun X. Superior energy capacity of graphene nanosheets for a nonaqueous lithium–oxygen battery. Chem Comm 2011;33(47):9438–40.

[12] Yoo E, Zhou H. Li–air rechargeable battery based on metal-free graphene nanosheet catalysts. ACS Nano 2011;5(4):3020–6.

[13] Xiao J, Mei D, Li X, Xu W, Wang D, Graff G, et al. Hierarchically porous graphene as a lithium–air battery electrode. Nano Lett 2011;11(11):5071–8.

[14] Wang Y, Zhou H. To draw an air electrode of a Li–air battery by pencil. Energy Environ Sci 2011;5(4):1704–7.

[15] Li Y, Wang J, Li X, Geng D, Banis M, Li R, et al. Nitrogen-doped graphene nanosheets as cathode materials with excellent electrocatalytic activity for high capacity lithium–oxygen batteries. Electrochem Commun 2012;18:12–5.

[16] Li Y, Wang J, Li X, Geng D, Banis M, Tang Y, et al. Discharge product morphology and increased charge performance of lithium–oxygen batteries with graphene nanosheet electrodes: the effect of sulphur doping. J Mater Chem 2012;38(22):20170–4.

[17] Read J. Characterization of the lithium/oxygen organic electrolyte battery. J Electrochem Soc 2002;149(9):A1190–5.

[18] Viswanathan V, Thygesen K, Hummelshøj J, Nørskov J, Girishkumar G, McCloskey B, et al. Electrical conductivity in Li_2O_2 and its role in determining capacity limitations in non-aqueous Li–O_2 batteries. J Chem Phys 2011;135(21):214704.

[19] Albertus P, Girishkumar G, McCloskey B, Sànchez Carrera R, Kozinsky B, Christensen J, et al. Identifying capacity limitations in the Li/oxygen battery using experiments and modeling. J Electrochem Soc 2011;158(3):A343–51.

[20] Given PH. Coal Science. Washington DC: American Chemical Society; 1966.

[21] Jaouen F, Dodelet JP. Non-noble electrocatalysts for O_2 reduction: how does heat treatment affect their activity and structure? Part I. model for carbon black gasification by NH_3: parametric calibration and electrochemical validation. J Phys Chem C 2007;111(16):5963–70.

[22] Jaouen F, Serventi A, Lefèvre M, Dodelet J, Bertrand P. Non-noble electrocatalysts for O_2 reduction: how does heat treatment affect their activity and structure? Part II. structural changes observed by electron microscopy, raman, and mass spectroscopy. J Phys Chem C 2007;111(6):5971–6.

[23] Lefèvre M, Dodelet JP. Fe-based electrocatalysts made with microporous pristine carbon black supports for the reduction of oxygen in PEM fuel cells. Electrochim Acta 2008;53(28):8269–76.

[24] Charreteur F, Jaouen F, Dodelet JP. Iron porphyrin-based cathode catalysts for PEM fuel cells: Influence of pyrolysis gas on activity and stability. Electrochim Acta 2009;54(26):6622–30.

[25] Lu Y, Gallant B, Kwabi D, Harding J, Mitchell R, Whittingham M, et al. Lithium–oxygen batteries: bridging mechanistic understanding and battery performance. Energy Environ Sci 2013;6:750–68.

[26] Adams B, Radtke C, Black R, Trudeau M, Zaghib K, Nazar L. Current density dependence of peroxide formation in the Li–O_2 battery and its effect on charge. Energy Environ Sci 2013;6:1772–8.

[27] McCloskey B, Speidel A, Scheffler R, Miller D, Viswanathan V, Hummelshøj J, et al. Twin problems of interfacial carbonate formation in nonaqueous Li–O_2 batteries. J Phys Chem Lett 2012;3:997–1001.

[28] Thotiyl M, Freunberger S, Peng Z, Bruce P. The carbon electrode in nonaqueous Li–O_2 cells. J Am Chem Soc 2013;135(1):494–500.

[29] Chen Y, Freunberger S, Peng Z, Fontaine O, Bruce P. Charging a Li–O_2 battery using a redox mediator. Nat Chem 2013;5:489–94.

[30] Li F, Zhang T, Zhou H. Challenges of non-aqueous Li–O_2 batteries: electrolytes, catalysts, and anodes. Energy Environ Sci 2013;6:1125–41.

[31] Black R, Oh S, Lee J, Yim T, Adams B, Nazar L. Screening for superoxide reactivity in Li–O_2 batteries: effect on Li_2O_2/LiOH crystallization. J Am Chem Soc 2012;134:2902–5.

[32] Mitchell R, Gallant B, Shao-Horn Y, Thompson C. Mechanisms of morphological evolution of Li_2O_2 particles during electrochemical growth. J Phys Chem Lett 2013;4:1060–4.

[33] Hummelshøj J, Blomqvist J, Datta S, Vegge T, Rossmeisl J, Thygesen K, et al. Communications: elementary oxygen electrode reactions in the aprotic Li–air battery. J Chem Phys 2010;132:071101.

[34] Meini S, Piana M, Tsiouvaras N, Garsuch A, Gasteiger H. The effect of water on the discharge capacity of a non-catalyzed carbon cathode for Li–O_2 batteries. Electrochem Solid-State Lett 2012;15(4):A45–8.

[35] Lu Y, Gasteiger H, Shao-Horn Y. Method development to evaluate the oxygen reduction activity of high-surface-area catalysts for Li–air batteries. Electrochem Solid-State Lett 2011;14(5):A70–4.

[36] Meini S, Piana M, Beyer H, Schwämmlein J, Gasteiger H. Effect of carbon surface area on first discharge capacity of Li–O_2 cathodes and cycle-life behavior in ether-based electrolytes. J Electrochem Soc 2012;159(12):A2135–142.

[37] Black R, Oh S, Lee J, Yim T, Adams B, Nazar L. Screening for superoxide reactivity in Li–O_2 batteries: effect on Li_2O_2/LiOH crystallization. J Am Chem Soc 2012;134(6):2902–5.

[38] Sadezky A, Muckenhuber H, Grothe H, Niessner R, PöSchl U. Raman microspectroscopy of soot and related carbonaceous materials: spectral analysis and structural information. Carbon 2005;43(8):1731–42.

[39] Charreteur F, Jaouen F, Ruggeri S, Dodelet JP. Fe/N/C non-precious catalysts for PEM fuel cells: influence of the structural parameters of pristine commercial carbon blacks on their activity for oxygen reduction. Electrochim Acta 2008;53(6):2925–38.